NANO LETTERS

pubs.acs.org/NanoLett Letter

Unravelling Ultrafast Li Ion Transport in Functionalized Metal–Organic Framework-Based Battery Electrolytes

Guorui Cai,[#] Amanda A. Chen,[#] Sharon Lin, Dong Ju Lee, Kunpeng Yu, John Holoubek, Yijie Yin, Anthony U. Mu, Ying Shirley Meng, Ping Liu, Seth M. Cohen,[*] Tod A. Pascal,[*] and Zheng Chen[*]

Cite This: https://doi.org/10.1021/acs.nanolett.3c01825 Read Online

ACCESS | Metrics & More | Article Recommendations | Supporting Information

ABSTRACT: Nonaqueous fluidic transport and ion solvation properties under nanoscale confinement are poorly understood, especially in ion conduction for energy storage and conversion systems. Herein, metal–organic frameworks (MOFs) and aprotic electrolytes are studied as a robust platform for molecular-level insights into electrolyte behaviors in confined spaces. By employing computer simulations, along with spectroscopic and electrochemical measurements, we demonstrate several phenomena that deviate from the bulk, including modulated solvent molecular configurations, aggregated solvation structures, and tunable transport mechanisms from quasi-solid to quasi-liquid in functionalized MOFs. Technologically, taking advantage of confinement effects may prove useful for addressing stability concerns associated with volatile organic electrolytes while simultaneously endowing ultrafast transport of solvates, resulting in improved battery performance, even at extreme temperatures. The molecular-level insights presented here further our understanding of structure–property relationships of complex fluids at the nanoscale, information that can be exploited for the predictive design of more efficient electrochemical systems.

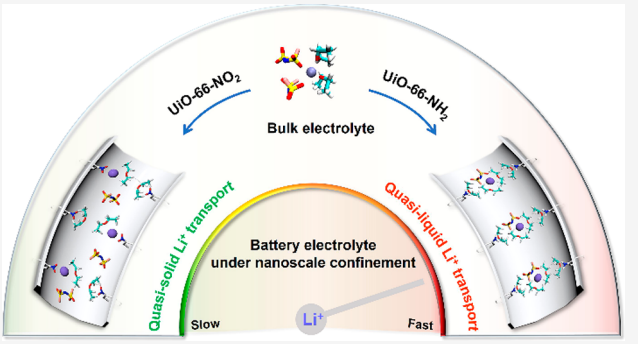

KEYWORDS: *ion transport, ion solvation, nanoconfinement, metal–organic frameworks, extreme temperatures*

Emerging nanotechnologies are increasingly drawing inspiration from living systems,[1] including recent efforts exploiting ultrafast flow through carbon nanochannels, correlated ion transport, sharply decreased dielectric permittivity of confined water, and selective ion separation.[2−6] The primary focus on aqueous systems has led to technological advances encompassing artificial ion channels and osmotic energy harvesting as well as two-dimensional membranes. Equally interesting, yet much less explored, are the transport properties of nonaqueous liquids, such as organic electrolyte solvents with dissolved ionic species.

We are fundamentally interested in understanding the molecular mechanisms that underlie the operation of electrochemical cells, primarily lithium ion batteries (LIBs). Recent efforts have focused on electrolyte design as a means of engineering batteries that are finely tuned for specific applications, such as low-temperature operations.[7−12] Some of the most promising technologies comprise lithium metal anodes and liquid electrolytes; however, widespread adoption has been limited by the irregular transport of ions, uneven Li deposition, and low Coulombic efficiency (CE). Moreover, uncontrolled growth of sharp Li dendrites presents safety concerns since these dendrites can puncture the separator during long-term charge and discharge. The fact that commercial liquid electrolytes are volatile and flammable presents further challenges.[13,14]

Apart from the safety concerns, commercial LIBs show significant performance degradation at low temperatures, primarily due to the relatively high melting point of their liquid electrolytes,[15] which leads to high impedance (and even freezing) at low temperatures and, thus, significantly retarded ion transport. Cognizant of this reality, engineered electrolytes with low melting point solvents have been proposed and demonstrated as an excellent strategy to improve low-temperature performances.[16−19] For example, a carboxylic ester was used to replace the carbonate ester. Their low melting point and low solubility of polysulfides allow the Li–S half cells to be stable cycling at −40 °C while a mediocre Li metal CE at subzero temperatures.[20] Although the ethers with a high lowest unoccupied molecular orbital energy (LUMO) generally have a higher Li metal compatibility than common esters, the multidentate ethers encountered dendritic Li metal

Received: May 16, 2023
Revised: July 21, 2023

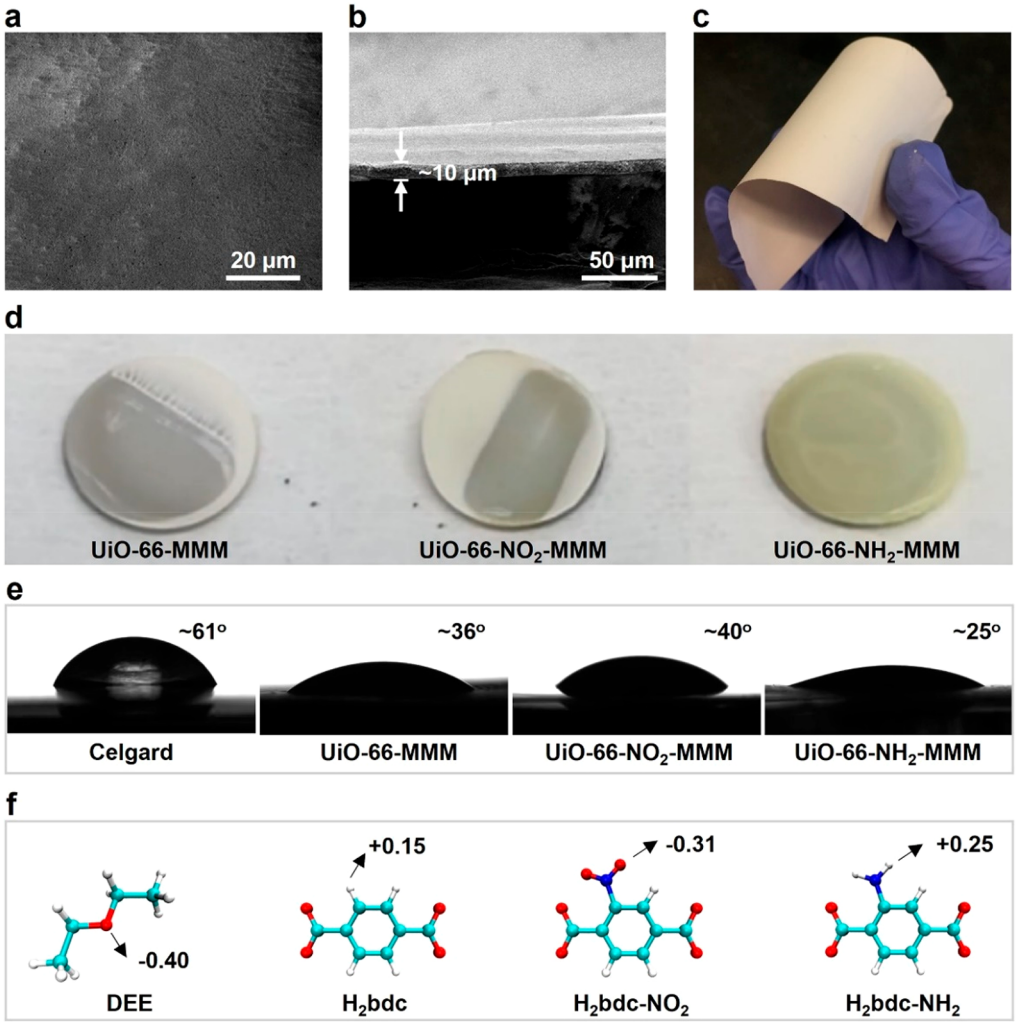

Figure 1. MOF-based mixed matrix membranes (MMMs). (a) Top and (b) cross-sectional SEM views and (c) digital photograph of representative MMMs. (d) Wettability testing of selected MMMs toward 1 M LiFSI DEE electrolyte. (e) Contact angle testing of 4 M LiFSI DEE on MMMs. (f) Atomistic representation of DEE and functionalized linker in MOFs. The partial atomic charges of the main interaction sites are labeled.

growth at low-temperature conditions.[21] The monodentate ether electrolytes comprising diethyl ether (DEE), which has a low melting point of −116 °C and high Li metal compatibility, enable reversible LIBs with good performance even at −60 °C.[22] One of our contributions to this field has been to determine that the underlying reason for this improved electrochemical performance of DEE is the undercoordinated ion-pairing solvation structure and weak Li^+-solvent binding, which allow facile low-temperature kinetics. However, low-melting-point solvents such as DEE generally also have low boiling points and are volatile and flammable, which presents additional safety concerns, especially at and above ambient temperatures (Video S1).

Capillary condensation of volatile gases in nanopores, where they liquify at pressures below their vapor pressure, is an alternative electrolyte engineering approach that has shown great potential.[23−25] Here, the trapped, liquified gas can deliver exceptionally high capacity at low pressures and temperatures, a considerable achievement because the state-of-the-art commercial Celgard membranes fail under these conditions.[25] However, although porous materials can trap the electrolyte and thereby alleviate the issue of evaporation of volatile solvents, this confinement results in strong friction between the nanopore walls and the electrolyte molecules, leading to high diffusion resistance, high overpotential, and inhomogeneous Li plating.[26−29] Thus, simultaneously achieving fast transport kinetics, high energy densities, and a wide-temperature operating window is currently not achievable. In this contribution, we overcome all these challenges while simultaneously advancing our understanding of the role of nanopore chemistry and morphology in facilitating ion transport.

To characterize the physicochemical and electrochemical properties of confined electrolytes at a molecular level, MOFs were selected as a model material, because of their high crystallinity, porous structure, design flexibility, and framework tunability.[30−34] Due to their high chemical and thermal stability, the UiO-66 series were selected as the porous host (Figure S1).[35] These MOFs are synthesized by the assembly of Zr^{4+} ions and terephthalic acid (H_2bdc) linkers. The resulting MOFs show a high specific Brunauer−Emmett−Teller (BET) surface area and small (~1.0 nm) nanocages with even smaller windows (~0.6 nm) (Figure S2), which is desirable for achieving strong nanoscale confinement effects. The pore morphology can be further engineered by modifying the linker group chemistry, i.e., replacing H_2bdc with different function-

https://doi.org/10.1021/acs.nanolett.3c01825
Nano Lett. XXXX, XXX, XXX−XXX

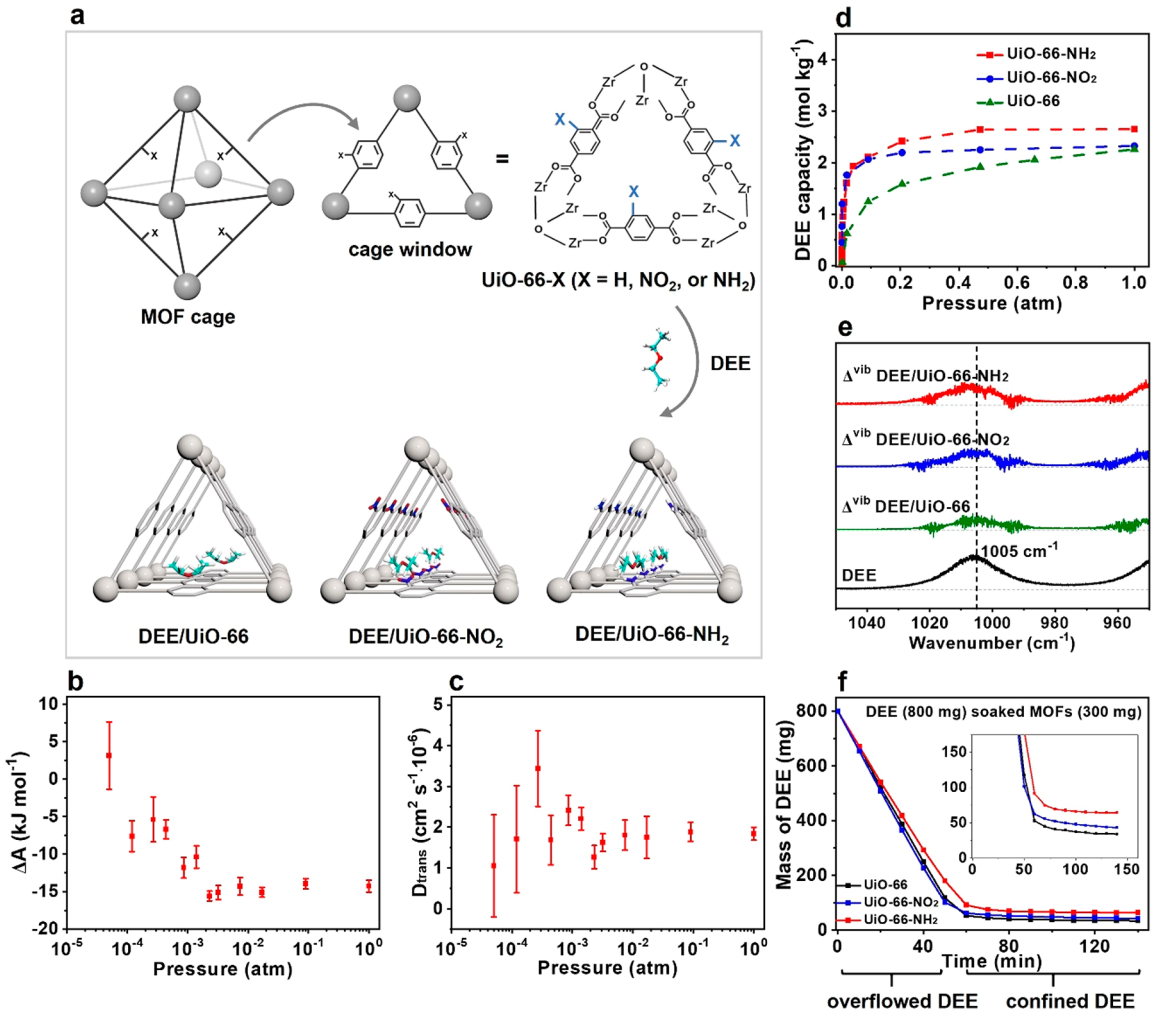

Figure 2. Microscopic signatures of MOF/DEE Interactions. (a) Schematic showing the MOF cage and the preferred DEE configurations in different MOF pores. (b) Calculated transfer free energy per DEE from the bulk into UiO-66-NH_2 pores. (c) DEE self-diffusion coefficient in UiO-66-NH_2 at 298 K. The uncertainty in our calculations is indicated by error bars. (d) GCMC simulation of DEE adsorption in MOFs at 298 K. (e) Simulated vibrational density of states (vDoS, i.e., spectral density) difference between DEE-soaked MOFs and corresponding empty MOFs. The vDoS of bulk DEE is given as a reference. (f) Experimental mass change of overflowed DEE-soaked MOF powders.

alized ligands (Figure S1). Lithium bis(fluorosulfonyl)imide (LiFSI) dissolved in DEE was used as the electrolyte, because of its high Li metal compatibility and superior low-temperature performance.[22]

Leveraging the remarkable capillary condensation and modulated microenvironment of MOFs, we hypothesized that these materials could trap DEE, thereby addressing safety concerns and enabling an even wider range of working temperatures. We further hypothesized that the introduction of chemical interactions, such as hydrogen bonding and Lewis acid−base coordination, could allow us to "dial-in" the trapping and transport ability of these MOFs toward confined volatile electrolytes, while concurrently facilitating Li^+ ion diffusion.

MOF-based mixed matrix membranes (MMMs) were fabricated based on a reported process (see the Supporting Information Section 1.2 and Figure S3).[36,37] UiO-66-MMMs (Figure S4) were characterized by scanning electron microscopy (SEM, Figure 1a,b), showing a compacted and thin (~10 μm) membrane structure. The resulting membrane was found to be quite flexible (Figure 1c) and stable in common electrolyte systems (Figure S5). Similarly, other MMMs, based on UiO-66-NH_2 or UiO-66-NO_2, were also fabricated using an identical method, and presented robust stability in common electrolytes even at 50 °C (Figures S6 and S7). In addition, the N_2 sorption testing was conducted to assess the porosity of both commercial membranes and our MMMs (Figure S8). The total pore volume of UiO-66-NH_2-MMM was found to be lower compared to Celgrad 2500 (0.616 vs 0.858 $cm^3\ g^{-1}$). This characteristic is particularly advantageous, as it helps reduce the amount of electrolyte required to wet separators.

The feasibility of MMMs working as battery separators was evaluated by wettability testing in 1 M LiFSI DEE electrolyte (Video S2). We found that the UiO-66-NH_2-MMMs were fully wet immediately upon dropping on the electrolyte, while a longer wet time was needed for the UiO-66-MMMs and UiO-66-NO_2-MMMs (Figure 1d), which suggests different electrolyte transport kinetics. Contact angle measurements (Figure 1e) showed low contact angles for the electrolyte solution on the MMMs, in contrast to the relatively high contact angle (~61°) measured on Celgard membranes. The contact angle varied for UiO-66-NH_2 (~25°) and UiO-66-NO_2 (~40°)

https://doi.org/10.1021/acs.nanolett.3c01825
Nano Lett. XXXX, XXX, XXX−XXX

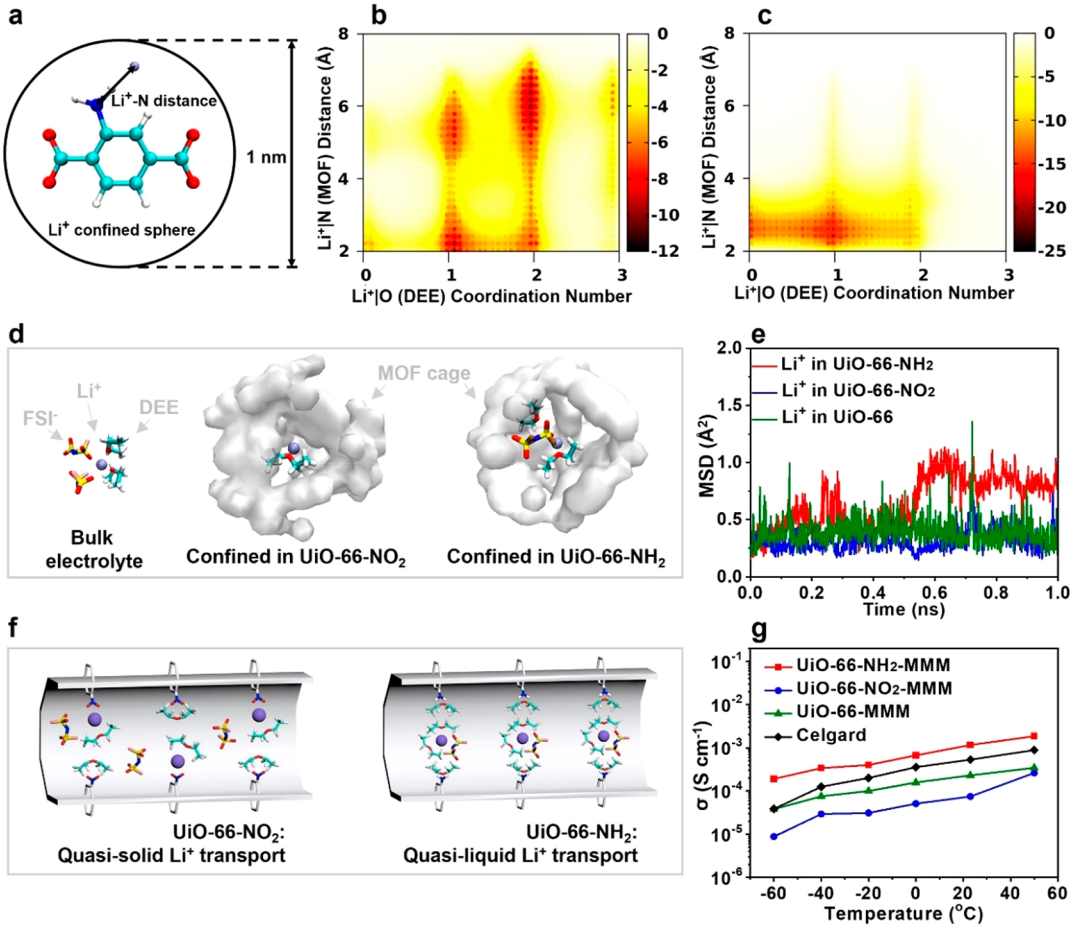

Figure 3. Confined solvated Li^+ structure and transport. (a) Schematic of the accelerated MD simulations to obtain the Li^+ 2D free energy surface (FES). (b) 2D FES of Li^+ in UiO-66-NH_2 and (c) UiO-66-NO_2. The color scheme goes from white (less favorable) to black (more favorable). (d) Snapshots of the representative solvation structures for Li^+ inside UiO-66-NH_2, UiO-66-NO_2, and bulk electrolytes. (e) Li^+ Mean Square Displacement (MSD) calculations inside UiO-66-NH_2, UiO-66, and UiO-66-NO_2. The result shows two regimes of Li^+ diffusion: Quasi-solid hopping in UiO-66, and UiO-66-NO_2 compared to quasi-liquid in UiO-66-NH_2. (f) Schematic showing the Li^+ ion migration pathway inside UiO-66-NH_2 and UiO-66-NO_2. (g) Ionic conductivity of 1 M LiFSI DEE electrolytes confined in selected MMMs or Celgard membranes.

MMMs (Figure 1f), which is likely reflective of the DEE solvent interactions with the polar groups in these MOFs.

Microscopic insights into the MOF/DEE interactions were obtained by calculating the DEE/MOF-linker potential energy surface by means of quantum mechanical (QM) electronic structure calculations of representative model systems (Supporting Information Section 2.2). We found significant modulation of the binding energy of DEE to the various linker groups depending on the binding geometry (Table S2, Figure 2a). To facilitate more extensive simulations at finite temperature, we developed a classical force field based on these QM results (Table S3). We then determined the free energy of transferring a DEE molecule from the bulk liquid into UiO-66-NH_2, as a function of applied pressure (Figure 2b), using equilibrium molecular dynamics (MD) simulations (see the Supporting Information Section 2.4). These revealed a large initial slope in the free energy (i.e., a favorable chemical potential) of transfer and thus an appreciable thermodynamic driving force for DEE infiltration into the UiO-66-NH_2. The chemical potential eventually converged to 0 to ∼0.002 atm, which represents the saturation limit. At this point, we found that each DEE molecule is on average $\Delta G = (G_{MOF} - G_{bulk}) = \Delta H - T\Delta S = -14.7$ kJ/mol more stable inside UiO-66-NH_2 than in the bulk liquid, which is driven by increased enthalpy $\Delta H = -36.3$ kJ/mol and opposed by reduced entropy $T\Delta S = -21.5$ kJ/mol (Table S4). Moreover, free energy results indicate that at this saturation limit, each DEE molecule inside the UiO-66-NH_2 is −50.6 kJ/mol more stable than that in the gas phase, corresponding to a ∼50-fold decrease in the vapor pressure compared to the bulk liquid (see the Supporting Information Section 2.4).

The enhanced thermodynamic stability of DEE inside the MOF manifests concomitant transport properties. Figure 2c shows a plot of the calculated DEE self-diffusion constant, which, in the case of UiO-66-NH_2, shows a change in slope between 0.0001 and 0.001 atm, indicative of a phase transition. We classify the DEE "phase" before this transition as that of largely immobilized molecules that infrequently hop from one site to another, which we term a "quasi-solid" phase. After the phase transition, the DEE more closely resembles a "quasi-liquid" phase, with self-diffusion that much more closely resembles that of a confined fluid. Of note, the predicted phase transition pressure is significantly lower than the gas → liquid transition pressure (∼0.7 atm) for bulk DEE, i.e., is a signature of capillary condensation.

We also considered the thermodynamics of DEE infiltration into the parent UiO-66 and UiO-66-NO_2, in Figures S9 and S10. We found that the ability of UiO-66 to confine DEE

https://doi.org/10.1021/acs.nanolett.3c01825
Nano Lett. XXXX, XXX, XXX−XXX

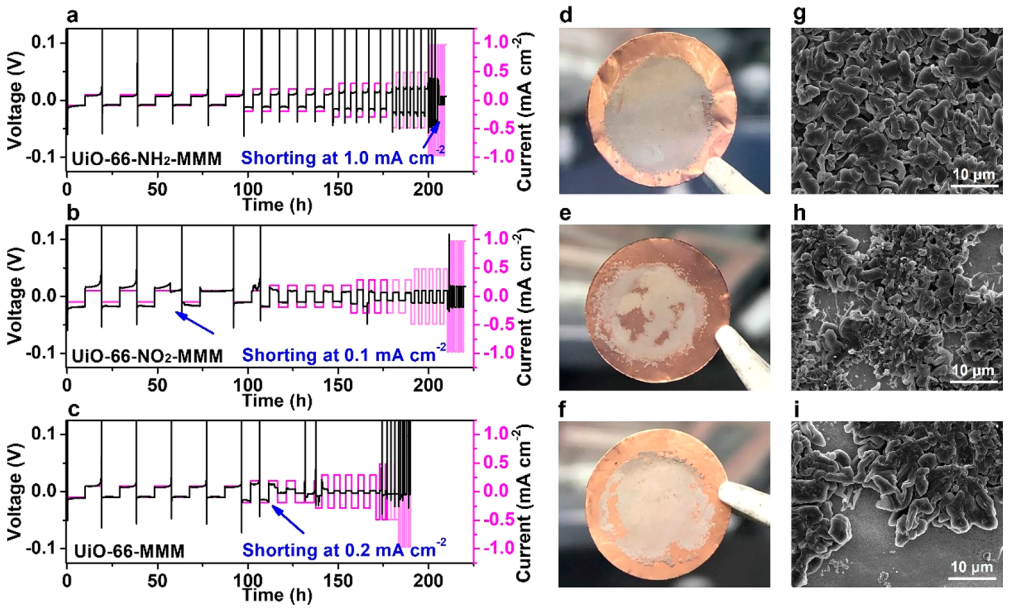

Figure 4. Li metal plating/stripping behaviors. (a–c) The critical current density testing of Li//Cu cells using different MMMs as the separator. (d–f) Digital photographic and (g–i) SEM images of deposited Li metal on copper foil by using (d, g) UiO-66-NH_2, (e, h) UiO-66, and (f, i) UiO-66-NO_2-MMMs as the separators.

molecules is much weaker than that of both UiO-66-NH_2 and UiO-66-NO_2. These results are consistent with isothermal adsorption curves obtained from Grand Canonical Monte Carlo (GCMC) calculations (see the Supporting Information Section 2.3) where, in terms of the adsorption capability, we find UiO-66-NH_2 > UiO-66-NO_2 > UiO-66 (Figure 2d).

Experimental signatures of the DEE/MOF microstructure interactions were obtained by Fourier-transform infrared spectroscopy (FTIR) spectroscopy, which showed the characteristic peak of DEE in the soaked MOFs (Figure S11). We found a slight red shift of ∼29 cm^{-1} in a peak at 1106 cm^{-1}, indicative of chemical interactions, possibly due to hydrogen bonding and Lewis acid–base coordination. To fingerprint the microscopic interactions responsible for this peak, we performed additional computer simulations and calculated the vibrational density of states (vDoS or spectral density) function, which showed enhancements in a peak near 1005 cm^{-1} (Figure 2e) due to C–O stretching (Figure S12). We note that the difference in the peak energies between the simulations and experiments results primarily from the unoptimized valence interactions in our force field. While this can be resolved by careful reparameterization, it is not expected to materially change the results presented here. To further validate our simulations, and particularly the predicted DEE uptake capabilities and reduced vapor pressure of the MOFs, we performed soaking experiments using activated MOF samples (300 mg) and an excess of 800 mg of DEE. The mass change of DEE was measured under ambient pressure in an argon-filled glovebox. Although the bulk DEE evaporates within a few minutes, we found that confined DEE in the MOFs remains stable for nearly 2 h with no appreciable reduction in mass (Figure 2f).

Both our simulations and experiments confirm the initial hypothesis that MOFs can adsorb and trap volatile electrolytes, thereby potentially addressing the safety concerns of these flammable solvents. We then considered the transport properties of dissolved ions and hypothesized that the ion–MOF interactions could be tailored to achieve fast ion diffusion and improved electrochemical performance.

We obtained detailed structural information about the local Li^+ ion solvation environment in a 1 M LiFSI DEE electrolyte and infiltrated in the functionalized MOFs from additional equilibrium MD simulations. We found that the Li^+ ions in UiO-66-NH_2 had a comparable Li^+|O(DEE) coordination number (average coordination number 1.75) when compared to bulk electrolyte that is greater than that of UiO-66 or UiO-66-NO_2 (average coordination numbers 1.5 and 0.83, respectively) (Figure S13a). Inside the MOFs, mostly due to steric effects, the ion-pairing (i.e., the Li^+ ion coordination with the O on FSI^-) is significantly reduced, with calculated coordination numbers of 0.84 in UiO-66-NH_2, 0.52 in UiO-66 and 0.18 in UiO-66-NO_2, compared to 2.96 in the bulk (Figure S13b). More details of the radial distribution functions and coordination numbers were shown in Figure S13c,d and Figure S14. To quantify the Li^+ free energy surface, we performed advanced sampling MD simulations using the 2D-Metadynamics approach, where we monitored the Li^+|O(DEE) coordination number and the Li^+|N(MOF-linker) distance (Figure 3a). These simulations revealed a free energy minimum for fully solvated Li^+ ions in the center of the channel in the case of UiO-66-NH_2, whereas the Li^+ ions are preferentially absorbed near the $-NO_2$ group in UiO-66-NO_2 (Figure 3b,c). Representative snapshots of the solvation structures for confined electrolytes and bulk electrolytes are shown in Figure 3d and Figure S15.

Further support for our free energy surfaces was obtained by calculating the Li^+ self-diffusion constant via Einstein's eq (Figure 3e and Figure S16). These calculations reveal a quasi-solid (in the case of UiO-66 and UiO-66-NO_2) versus a quasi-liquid (UiO-66-NH_2) diffusion mechanism. A schematic of Li^+ ion migration through the MOFs is shown in Figure 3f. Here, the solvent coordinated Li^+ ions in UiO-66-NH_2 are electrostatically shielded from the MOF linker; thus, their transport is dictated primarily by the diffusion of the DEE solvent. In contrast, the undercoordinated Li^+ in UiO-66 and

https://doi.org/10.1021/acs.nanolett.3c01825
Nano Lett. XXXX, XXX, XXX–XXX

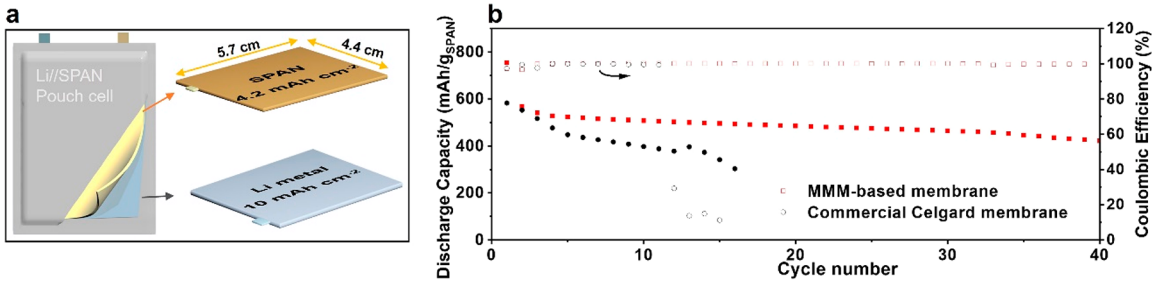

Figure 5. Full cell performance. (a) Schematic showing the assembly and parameter of the pouch cells. (b) Cycling performance of Li//SPAN pouch cells with bulk and UiO-66-NH_2-MMMs confined electrolytes.

UiO-66-NO_2 more strongly interacts with the MOF linker group, and their transport is dictated by a hopping mechanism where each Li^+ must overcome a significant barrier to go from site to site, as in a solid-state ion conductor. The significant reduction in the Li^+ diffusion constant in UiO-66-NO_2, due to the strong linker-undercoordinated Li^+ group interactions and concomitantly the reduced solvent coordination environment, is predicted to thus lead to significantly reduced conductivity in this system.

To test these computational predictions, we performed experimental ionic conductivity measurement of MMMs soaked in 1 M LiFSI DEE electrolyte. These measurements confirmed that UiO-66-NH_2-MMMs deliver superior conductivity compared with the two other MOF-MMMs (Figure 3g). The highly ordered pore structures in UiO-66-NH_2 and preferred orientation of trapped solvents play critical roles in inducing a well-aligned diffusion of the solvates. The driving force of directed solvated Li^+ ion diffusion and quasi-liquid diffusion mechanisms synergistically allows a higher ion conductivity than those in the bulk liquids with a random ion diffusion (Figures 2a and 3f). Indeed, we found that UiO-66-NH_2-MMMs had a higher conductivity than that of the bulk electrolytes with a commercial Celgrad membrane separator. Thus, the quasi-liquid diffusion mechanisms proposed here are distinct from conventional porous confined electrolytes that rely on the ion hopping mechanisms that result in a sluggish ion transport compared with the bulk liquids.

To understand the effects of chemical moieties in MOFs on LMB cyclability, the critical current density was evaluated (Figure 4a–c). Using UiO-66-NH_2-MMMs as the separator of Li//Cu cells allowed for operation at currents as high as 0.5 mA cm^{-2}. By contrast, cells with UiO-66-NO_2 and UiO-66 groups suffered from soft-shorting issues when the current densities reached 0.1 and 0.2 mA cm^{-2}, respectively. This can be attributed to UiO-66-NH_2 with sufficient Li^+ ion flux, as discussed previously. The effect of MOF composition toward the morphology of the deposited lithium was subsequently investigated. After applying 0.5 mA cm^{-2} current for 2 h, the cells were disassembled, and the electrodeposited lithium on the copper foils was characterized. Both macroscopic (Figure 4d–f) and microscopic (Figure 4g–i) images of UiO-66-MMMs and UiO-66-NO_2-MMMs systems showed sparse Li deposits. It is thus concluded that UiO-66 and UiO-66-NO_2 promote dendritic Li growth, while UiO-66-NH_2 produces more uniform morphologies and thus is potentially viable for the long-term lithium metal anode cycling.

To investigate the influence of the temperature on the kinetics and stability of the MMM-trapped electrolyte systems, we performed long-term lithium cycling tests in a wide-temperature range. As shown in Figure S17, the cells with MMMs and 1 M LiFSI DEE maintained stable Li plating and stripping at 50, 23, −40, and −60 °C. The impedance of the cell significantly increased with decreasing temperature, resulting in slightly higher overpotential and reduced CEs. We further studied the MMMs in pouch cells with Li metal as the anode and sulfurized polyacrylonitrile (SPAN) as the cathode (Figure 5). Cells using MMM-based membrane were found to stably cycle at room temperature, maintaining more than 70% capacity retention after 40 cycles, whereas cells using Celgard membrane failed after 12 cycles due to the rapid evaporation of the DEE solvent from the bulk electrolyte. To further examine the merits of our MMMs trapped volatile electrolytes, the Li//SPAN cells with several common electrolytes were also assembled (Figure S18). The coin cells with carbonate-based electrolytes, e.g., 1 M $LiPF_6$ ethylene carbonate (EC)/diethyl carbonate (DEC), showed poor long-term cycling due to their low Li metal compatibility. Although decent Li metal CEs can be expected for the ether-based electrolytes, e.g., 1 M LiTFSI 0.2 M $LiNO_3$ in 1,3-dioxolane (DOL)/dimethoxyethane (DME) (1/1 in volume), they displayed poor SPAN cycling stability due to their high solubility toward polysulfides. This was particularly apparent at reduced temperatures, where cells with conventional ether and carbonate electrolytes showed nearly no capacity. In contrast, the high Li metal compatibility and the superior transport properties at a wide-temperature range of the MMM-trapped DEE (Figure 3 and Figure S17) allowed these cells to stably cycle at both 23 and −40 °C.

In summary, the nonaqueous fluidic transport and ion solvation properties of aprotic electrolytes under confinement were evaluated using MOFs with different functional groups as the porous host. Both experiments and computational simulations showed a strong trapping ability of MOFs toward volatile electrolyte solvents, which addresses the stability concerns caused by volatile and flammable electrolytes. In addition, we found unique solvation structures and a quasi-liquid transport mechanism in UiO-66-NH_2, which led to significantly improved battery performance. This establishes new design principles for optimizing future electrochemical devices with tunable solvent and ion coordination properties over a wide temperature range. This work also provides molecular level understanding of the liquid electrolyte behaviors in nanoconfined environments and related charge transport behavior on functional electrochemical devices.

https://doi.org/10.1021/acs.nanolett.3c01825
Nano Lett. XXXX, XXX, XXX−XXX

■ ASSOCIATED CONTENT

Supporting Information

The Supporting Information is available free of charge at https://pubs.acs.org/doi/10.1021/acs.nanolett.3c01825.

Violability testing of DEE and common electrolyte solvents (MP4)

Wettability testing of MMMs with different functionalized MOFs toward 1 M LiFSI DEE (MP4)

Experimental methods, computational details, tables of densities and entropies, energies, and thermodynamics, figures of crystal structures, sorption isotherms and pore size distributions, fabrication process, photographs of UiO-66-MMM, XRD patterns, energy differences, diffusion coefficients, IR spectra, DOS, and Li coordination with O and N, Radial distribution functions, MD snapshots, ion transport, wide-temperature testing, and cycling testing (PDF)

■ AUTHOR INFORMATION

Corresponding Authors

Seth M. Cohen − *Department of Nano and Chemical Engineering, University of California, San Diego, La Jolla, California 92093, United States; Department of Chemistry and Biochemistry, University of California, San Diego, La Jolla, California 92093, United States;* orcid.org/0000-0002-5233-2280; Email: scohen@ucsd.edu

Tod A. Pascal − *Department of Nano and Chemical Engineering, University of California, San Diego, La Jolla, California 92093, United States; Department of Chemistry and Biochemistry, Program of Materials Science and Engineering, and Sustainable Power and Energy Center, University of California, San Diego, La Jolla, California 92093, United States;* orcid.org/0000-0003-2096-1143; Email: tpascal@ucsd.edu

Zheng Chen − *Department of Nano and Chemical Engineering, University of California, San Diego, La Jolla, California 92093, United States; Department of Chemistry and Biochemistry, Program of Materials Science and Engineering, and Sustainable Power and Energy Center, University of California, San Diego, La Jolla, California 92093, United States;* orcid.org/0000-0002-9186-4298; Email: zhengchen@eng.ucsd.edu

Authors

Guorui Cai − *Department of Nano and Chemical Engineering, University of California, San Diego, La Jolla, California 92093, United States*

Amanda A. Chen − *Department of Nano and Chemical Engineering, University of California, San Diego, La Jolla, California 92093, United States;* orcid.org/0000-0002-7358-222X

Sharon Lin − *Department of Chemistry and Biochemistry, University of California, San Diego, La Jolla, California 92093, United States*

Dong Ju Lee − *Department of Nano and Chemical Engineering, University of California, San Diego, La Jolla, California 92093, United States*

Kunpeng Yu − *Department of Nano and Chemical Engineering, University of California, San Diego, La Jolla, California 92093, United States*

John Holoubek − *Department of Nano and Chemical Engineering, University of California, San Diego, La Jolla, California 92093, United States;* orcid.org/0000-0003-0015-4512

Yijie Yin − *Program of Materials Science and Engineering, University of California, San Diego, La Jolla, California 92093, United States*

Anthony U. Mu − *Department of Nano and Chemical Engineering, University of California, San Diego, La Jolla, California 92093, United States*

Ying Shirley Meng − *Department of Nano and Chemical Engineering, University of California, San Diego, La Jolla, California 92093, United States; Pritzker School of Molecular Engineering, University of Chicago, Chicago, Illinois 60637, United States;* orcid.org/0000-0001-8936-8845

Ping Liu − *Department of Nano and Chemical Engineering, University of California, San Diego, La Jolla, California 92093, United States; Department of Chemistry and Biochemistry, Program of Materials Science and Engineering, and Sustainable Power and Energy Center, University of California, San Diego, La Jolla, California 92093, United States;* orcid.org/0000-0002-1488-1668

Complete contact information is available at: https://pubs.acs.org/10.1021/acs.nanolett.3c01825

Author Contributions

#G.C. and A.A.C. contributed equally to this work.

Author Contributions

All authors have given approval to the final version of the manuscript.

Notes

The authors declare no competing financial interest.

■ ACKNOWLEDGMENTS

This work was primarily supported by the US National Science Foundation (NSF) through the UC San Diego Materials Research Science and Engineering Center (UCSD MRSEC), Grant No. DMR-2011924 (Z.C., T.A.P., and S.M.C.). The majority of cell fabrication and electrochemical testing was performed in the UCSD-MTI Battery Fabrication and the UCSD-Arbin Battery Testing Facility. This work was performed in part at the San Diego Nanotechnology Infrastructure (SDNI) of UCSD, a member of the National Nanotechnology Coordinated Infrastructure, which is supported by the National Science Foundation (Grant ECCS-1542148). T.A.P. acknowledges support from US Department of Energy (DOE), Basic Energy Science, Grant no. DE-SC0023503 and NSF Grant No. CBET- 309147. This research used resources of the National Energy Research Scientific Computing Center, a DOE Office of Science User Facility supported by the Office of Science of the U.S. DOE under Contract No. DE-AC02-05CH11231. This work also used CPU time at the San Diego Supercomputing Center through allocation DMR190106 from the Advanced Cyberinfrastructure Coordination Ecosystem: Services & Support (ACCESS) program, which is supported by NSF grants #2138259, #2138286, #2138307, #2137603, and #2138296.

■ REFERENCES

(1) Lynch, C. I.; Rao, S.; Sansom, M. S. Water in nanopores and biological channels: a molecular simulation perspective. *Chem. Rev.* **2020**, *120*, 10298−10335.

(2) Wang, M.; Zhang, P.; Liang, X.; Zhao, J.; Liu, Y.; Cao, Y.; Wang, H.; Chen, Y.; Zhang, Z.; Pan, F. Ultrafast seawater desalination with covalent organic framework membranes. *Nat. Sustain.* **2022**, *5*, 518−526.
(3) Chen, H.; Ran, T.; Gan, Y.; Zhou, J.; Zhang, Y.; Zhang, L.; Zhang, D.; Jiang, L. Ultrafast water harvesting and transport in hierarchical microchannels. *Nat. Mater.* **2018**, *17*, 935−942.
(4) Zhang, W.-H.; Yin, M.-J.; Zhao, Q.; Jin, C.-G.; Wang, N.; Ji, S.; Ritt, C. L.; Elimelech, M.; An, Q.-F. Graphene oxide membranes with stable porous structure for ultrafast water transport. *Nat. Nanotechnol.* **2021**, *16*, 337−343.
(5) Joshi, R.; Carbone, P.; Wang, F.-C.; Kravets, V. G.; Su, Y.; Grigorieva, I. V.; Wu, H.; Geim, A. K.; Nair, R. R. Precise and ultrafast molecular sieving through graphene oxide membranes. *Science* **2014**, *343*, 752−754.
(6) Nair, R.; Wu, H.; Jayaram, P. N.; Grigorieva, I. V.; Geim, A. Unimpeded permeation of water through helium-leak-tight graphene-based membranes. *Science* **2012**, *335*, 442−444.
(7) Zhang, Q.; Ma, Y.; Lu, Y.; Li, L.; Wan, F.; Zhang, K.; Chen, J. Modulating electrolyte structure for ultralow temperature aqueous zinc batteries. *Nat. Commun.* **2020**, *11*, 4463.
(8) Gao, Y.; Rojas, T.; Wang, K.; Liu, S.; Wang, D.; Chen, T.; Wang, H.; Ngo, A. T.; Wang, D. Low-temperature and high-rate-charging lithium metal batteries enabled by an electrochemically active monolayer-regulated interface. *Nat. Energy* **2020**, *5*, 534−542.
(9) Xiao, P.; Luo, R.; Piao, Z.; Li, C.; Wang, J.; Yu, K.; Zhou, G.; Cheng, H.-M. High-performance lithium metal batteries with a wide operating temperature range in carbonate electrolyte by manipulating interfacial chemistry. *ACS Energy Lett.* **2021**, *6*, 3170−3179.
(10) Wang, Z.; Sun, Z.; Shi, Y.; Qi, F.; Gao, X.; Yang, H.; Cheng, H. M.; Li, F. Ion-dipole chemistry drives rapid evolution of Li ions solvation sheath in low-temperature Li batteries. *Adv. Energy Mater.* **2021**, *11*, 2100935.
(11) Lin, S.; Hua, H.; Lai, P.; Zhao, J. A multifunctional dual-salt localized high-concentration electrolyte for fast dynamic high-voltage lithium battery in wide temperature range. *Adv. Energy Mater.* **2021**, *11*, 2101775.
(12) Gupta, A.; Bhargav, A.; Manthiram, A. Tailoring Lithium Polysulfide Coordination and clustering behavior through cationic electrostatic competition. *Chem. Mater.* **2021**, *33*, 3457−3466.
(13) Wang, J.; Yamada, Y.; Sodeyama, K.; Watanabe, E.; Takada, K.; Tateyama, Y.; Yamada, A. Fire-extinguishing organic electrolytes for safe batteries. *Nat. Energy* **2018**, *3*, 22−29.
(14) Liu, K.; Liu, Y.; Lin, D.; Pei, A.; Cui, Y. Materials for lithium-ion battery safety. *Sci. Adv.* **2018**, *4*, No. eaas9820.
(15) Zhang, N.; Deng, T.; Zhang, S.; Wang, C.; Chen, L.; Wang, C.; Fan, X. Critical review on low-temperature Li-ion/metal batteries. *Adv. Mater.* **2022**, *34*, 2107899.
(16) Fan, X.; Ji, X.; Chen, L.; Chen, J.; Deng, T.; Han, F.; Yue, J.; Piao, N.; Wang, R.; Zhou, X.; Xiao, X.; Wang, C. All-temperature batteries enabled by fluorinated electrolytes with non-polar solvents. *Nat. Energy* **2019**, *4*, 882−890.
(17) Dong, X.; Lin, Y.; Li, P.; Ma, Y.; Huang, J.; Bin, D.; Wang, Y.; Qi, Y.; Xia, Y. High-energy rechargeable metallic lithium battery at −70 °C enabled by a cosolvent electrolyte. *Angew. Chem., Int. Ed.* **2019**, *58*, 5623−5627.
(18) Rustomji, C. S.; Yang, Y.; Kim, T. K.; Mac, J.; Kim, Y. J.; Caldwell, E.; Chung, H.; Meng, Y. S. Liquefied gas electrolytes for electrochemical energy storage devices. *Science* **2017**, *356*, No. eaal4263.
(19) Cai, G.; Holoubek, J.; Li, M.; Gao, H.; Yin, Y.; Yu, S.; Liu, H.; Pascal, T. A.; Liu, P.; Chen, Z. Solvent selection criteria for temperature-resilient lithium-sulfur batteries. *Proc. Natl. Acad. Sci. U.S.A.* **2022**, *119*, No. e2200392119.
(20) Cai, G.; Holoubek, J.; Xia, D.; Li, M.; Yin, Y.; Xing, X.; Liu, P.; Chen, Z. An ester electrolyte for lithium-sulfur batteries capable of ultra-low temperature cycling. *Chem. Commun.* **2020**, *56*, 9114−9117.
(21) Thenuwara, A. C.; Shetty, P. P.; McDowell, M. T. Distinct nanoscale interphases and morphology of lithium metal electrodes operating at low temperatures. *Nano Lett.* **2019**, *19*, 8664−8672.
(22) Holoubek, J.; Liu, H.; Wu, Z.; Yin, Y.; Xing, X.; Cai, G.; Yu, S.; Zhou, H.; Pascal, T. A.; Chen, Z. Tailoring electrolyte solvation for Li metal batteries cycled at ultra-low temperature. *Nat. Energy* **2021**, *6*, 303−313.
(23) Yang, Q.; Sun, P. Z.; Fumagalli, L.; Stebunov, Y. V.; Haigh, S. J.; Zhou, Z. W.; Grigorieva, I. V.; Wang, F. C.; Geim, A. K. Capillary condensation under atomic-scale confinement. *Nature* **2020**, *588*, 250−253.
(24) Grommet, A. B.; Feller, M.; Klajn, R. Chemical reactivity under nanoconfinement. *Nat. Nanotechnol.* **2020**, *15*, 256−271.
(25) Cai, G.; Yin, Y.; Xia, D.; Chen, A. A.; Holoubek, J.; Scharf, J.; Yang, Y.; Koh, K. H.; Li, M.; Davies, D. M.; Mayer, M.; Han, T. H.; Meng, Y. S.; Pascal, T. A.; Chen, Z. Sub-nanometer confinement enables facile condensation of gas electrolyte for low-temperature batteries. *Nat. Commun.* **2021**, *12*, 3395.
(26) Zeng, Q.; Wang, J.; Li, X.; Ouyang, Y.; He, W.; Li, D.; Guo, S.; Xiao, Y.; Deng, H.; Gong, W. Cross-linked chains of metal-organic framework afford continuous ion transport in solid batteries. *ACS Energy Lett.* **2021**, *6*, 2434−2441.
(27) Li, X.; Xu, P.; Tian, Y.; Fortini, A.; Choi, S. H.; Xu, J.; Tan, X.; Liu, X.; Chen, G.; Zhang, C. Electrolyte modulators toward polarization-mitigated lithium-Ion batteries for sustainable electric transportation. *Adv. Mater.* **2022**, *34*, 2107787.
(28) Chang, Z.; Yang, H.; Pan, A.; He, P.; Zhou, H. An improved 9 micron thick separator for a 350 Wh/kg lithium metal rechargeable pouch cell. *Nat. Commun.* **2022**, *13*, 6788.
(29) He, Y.; Qiao, Y.; Chang, Z.; Zhou, H. The potential of electrolyte filled MOF membranes as ionic sieves in rechargeable batteries. *Energy Environ. Sci.* **2019**, *12*, 2327−2344.
(30) Xu, Z.; Luo, T.; Lin, W. Nanoscale metal-organic layers for biomedical applications. *Acc. Mater. Res.* **2021**, *2*, 944−953.
(31) Idrees, K. B.; Li, Z.; Xie, H.; Kirlikovali, K. O.; Kazem-Rostami, M.; Wang, X.; Wang, X.; Tai, T.-Y.; Islamoglu, T.; Stoddart, J. F.; Snurr, R. Q.; Farha, O. K. Separation of aromatic hydrocarbons in porous materials. *J. Am. Chem. Soc.* **2022**, *144*, 12212−12218.
(32) Canossa, S.; Ji, Z.; Gropp, C.; Rong, Z.; Ploetz, E.; Wuttke, S.; Yaghi, O. M. System of sequences in multivariate reticular structures. *Nat. Rev. Mater.* **2023**, *8*, 331.
(33) Wang, H.-F.; Chen, L.; Pang, H.; Kaskel, S.; Xu, Q. MOF-derived electrocatalysts for oxygen reduction, oxygen evolution and hydrogen evolution reactions. *Chem. Soc. Rev.* **2020**, *49*, 1414−1448.
(34) Cai, G.; Yan, P.; Zhang, L.; Zhou, H.-C.; Jiang, H.-L. Metal-organic framework-based hierarchically porous materials: synthesis and applications. *Chem. Rev.* **2021**, *121*, 12278−12326.
(35) Kandiah, M.; Nilsen, M. H.; Usseglio, S.; Jakobsen, S.; Olsbye, U.; Tilset, M.; Larabi, C.; Quadrelli, E. A.; Bonino, F.; Lillerud, K. P. Synthesis and stability of tagged UiO-66 Zr-MOFs. *Chem. Mater.* **2010**, *22*, 6632−6640.
(36) Kalaj, M.; Bentz, K. C.; Ayala, S., Jr; Palomba, J. M.; Barcus, K. S.; Katayama, Y.; Cohen, S. M. MOF-polymer hybrid materials: from simple composites to tailored architectures. *Chem. Rev.* **2020**, *120*, 8267−8302.
(37) Datta, S. J.; Mayoral, A.; Murthy Srivatsa Bettahalli, N.; Bhatt, P. M.; Karunakaran, M.; Carja, I. D.; Fan, D.; Graziane, M.; Mileo, P.; Semino, R.; Maurin, G. Rational design of mixed-matrix metal-organic framework membranes for molecular separations. *Science* **2022**, *376*, 1080−1087.

https://doi.org/10.1021/acs.nanolett.3c01825
Nano Lett. XXXX, XXX, XXX−XXX